IEICE TRANS. ELECTRON., VOL.E106–C, NO.6 JUNE 2023

PAPER Special Section on Recent Progress in Organic Molecular Electronics

Effects of Potassium Doping on the Active Layer of Inverse-Structured Perovskite Solar Cells

Tatsuya KATO[†], **Yusuke ICHINO**[†], ***Nonmembers***, **Tatsuo MORI**[†], ***and*** **Yoshiyuki SEIKE**[†a)], ***Members***

SUMMARY In this report, solar cell characteristics were evaluated by doping the active layer $CH_3NH_3PbI_3$ ($MAPbI_3$) with 3.0 vol% and 6.0 vol% of potassium ion (KI) in an inverse-structured perovskite solar cells (PSCs). The Tauc plots of the absorbance characteristics and the ionization potential characteristics show that the top end of the valence band shifted by 0.21 eV in the shallow direction from −5.34 eV to −5.13 eV, and the energy band gap decreased from 1.530 eV to 1.525 eV. Also, the XRD measurements show that the lattice constant decreased from 8.96 Å to 8.93 Å when KI was doped. The decrease in the lattice constant indicates that a part of the A site is replaced from methylammonium ion (MAI) to KI. In the J-V characteristics of the solar cell, the mean value of J_{sc} improved from 7.0 mA/cm^2 without KI to 8.8 mA/cm^2 with 3.0 vol% of KI doped and to 10.2 mA/cm^2 with 6.0 vol% of KI doped. As a result, the mean value of power-conversion efficiency (PCE) without KI was 3.5%, but the mean value of PCE improved to 5.2% with 3.0 vol% of KI doped and to 4.5% with 6.0 vol% of KI doped. Thus, it has shown that it is effective to dope KI to $MAIPBI_3$, which serves as the active layer, even in the inverse-structured PSCs.

key words: *perovskite solar cells (PSCs), inverse-structure, potassium ion, dope*

1. Introduction

PSCs are flexible and light weighted with PCE comparable to silicon-based solar cells and are the most promising solar cells in recent years [1]–[10]. According to the Best Research-Cell Efficiency Chart published by the National Renewable Energy Laboratory, the maximum PCE of PSCs has reached 25.7% as of 2022 [11].

The structure of the perovskite crystal that serves as the active layer can be represented by the composition of ABX_3. This is a crystal structure containing a monovalent organic cation at each vertex of the cubic lattice, a monovalent halogen anion at each vertex of the internal regular octahedron, and a divalent metal cation at its center. The material composition of perovskite is important for improving PCE. Pang et al. improved the conversion efficiency by converting some of the monovalent cations at the A site of the perovskite crystal structure from methylammonium ion (MAI) to formamidinium ion (FAI) [12]. However, this method has a problem that when $FAPbI_3$ is fabricated, a fragile perovskite crystal called a δ layer, which absorbs weakly in the visible light region, is formed because FAI has a large ionic radius. The perovskite crystal with more α-phases, which has higher light absorption efficiency in the visible light region, has better PCE.

It has been reported that by substituting a part of MAI and FAI with cesium cations or rubidium cations, which are alkali metals with smaller ionic radii, the formation of the δ layer is prevented and the conversion efficiency improved [13]. However, rare metals such as cesium and rubidium are in low supply and are expensive materials, making the price of PSCs high. Therefore, Segawa et al. fabricated PSCs of ($FA_{0.85}MA_{0.15}Pb(I_{0.85}Br_{0.15})$) by substituting potassium ion (KI), which is also an alkali metal and inexpensive because it is abundant on earth, achieving a PCE of 20% [14]. Nam et al. fabricated PSCs having a sequential structure of FTO / bl-TiO_2 / Perovskite / Spiro-OMeTAD / Au, and aimed for high PCE and stability by using the perovskite layer as the $Cs_{0.925}K_{0.075}PbI_2Br$ structure. The mean value of PCE without KI was 8.2%, and the mean value of PCE with KI was 9.1%. Furthermore, they showed that the normalized PCE of the $CsPbI_2Br$ device gradually decreased, reaching half of the initial value in 72 hours, while the $Cs_{0.925}K_{0.075}PbI_2Br$ device maintained 80% of the initial value up to 120 hours [15]. Zhanga et al. fabricated PSCs with FTO / Compact TiO_2 / Mesoporous TiO_2 / Perovskite / Spiro-OMeTAD / Au structure and introduced potassium iodide complex (KI_3) as a new additive to the perovskite precursor solution by gas quenching method. The results showed broad spectral sensitivity, strong luminescence, and extended carrier lifetime due to halide exchange and defect passivation with I_2. Champion devices made from a mixture of KI and KI_3 precursors achieve a PCE of 21.2%, ignoring hysteresis due to the presence of potassium salts [16]. Kandori et al. fabricated PSCs with FTO / Compact TiO_2 / Mesoporous TiO_2 / Perovskite / Spiro-OMeTAD / Au structure using KI and FAI-doped perovskite solution, and showed that the device doped with KI 5% and FAI 31% had a maximum conversion efficiency of 13.53%. It has also been confirmed that by using the air blow method during the process, a highly symmetric (002) orientation is formed in the tetragonal perovskite crystal, and the unit cell volume increases according to the amount of FAI doped [17]. However, in these reports [14]–[17], all attempts to improve performance by doping the perovskite layer with KI are only evaluations using sequential structured PVCs. In this study, the properties of potassium iodide doped with MAI were evaluated. MAIs are perovskite layer precursors in inverse-structured PSCs and can be fabricated at low temperatures.

Manuscript received June 15, 2022.
Manuscript revised September 15, 2022.
Manuscript publicized January 18, 2023.

[†]The authors are with Graduate School of Engineering, Aichi Institute of Technology, Toyota-shi, 470–0392 Japan.
a) E-mail: y_seike@aitech.ac.jp

DOI: 10.1587/transele.2022OMP0004

2. Experimental

Figure 1 shows the structure of the prototype PVCs. Film was formed in a simple glove box in a nitrogen atmosphere at temperatures from 18°C to 40°C and humidity from 25% to 30%. A glass substrate with a sheet resistance of 15 Ω and an ITO film (manufactured by Luminescence Technology) (size 30 mm × 15 mm × 0.7 mm) is cleaned as follows: Immersed in an ultrasonic bath containing ultrapure water for 10 minutes, immersed in an ultrasonic bath containing Semicoclean 23 (Furuuchi chemical) for 10 minutes, immersed in an ultrasonic bath containing ultrapure water for 5 minutes, immersed in an ultrasonic bath containing acetone for 10 minutes, and then immersed in an ultrasonic bath containing 2-propanol for 10 minutes. After that, the substrate was dried on a hot plate (As-one, REXIM RSH-1DN) at 100°C for 10 minutes, followed by UV ozone treatment (Nippon Laser & Electronics Lab, UV-03 Clean) for 15 minutes. Next, poly (3, 4-ethylenedioxythiophene) polystyrene sulfonate (PEDOT: PSS) (Clevious Al4083), which is the hole transport layer, was spin-coated at 5,000 rpm for 30 seconds, and then annealing was performed at 130°C for 20 minutes in an electric furnace (Yamato, DX401).

Perovskite crystals with the structure of $CH_3NH_3PBI_2$ form a film by the reaction of MAI and lead iodide (PbI_2). We used a solvent engineering method [18]–[21] to form a perovskite layer that serves as a power generation layer. The solution of the precursor to form the perovskite layer was prepared by doping 691.5 mg of PbI_2 (Tokyo Chemical Industry) and 238.5 mg of MAI (Tokyo Chemical Industry) into the mixed solution of 945 μL of DMF (Sigma-Aldrich) and 106 μL of Dimethyl sulfoxide (DMSO) (Fujifilm Wako Pure Chemical) and stirring it for 30 minutes by an ultrasonic cleaner until there was no undissolved residue remained. After that, keep the solution warm on a hot plate at 70°C. 249 mg of potassium iodide KI (Fujifilm Wako Pure Chemical) and 1 mL of N, N-dimethylformamide (DMF)0.64 were mixed and kept warm overnight on a hot plate at 30°C. Three types of precursor solutions were prepared by doping 0 mL, 33 mL, and 67 mL of potassium iodide solution so that KI concentrations become 0 vol%, 3 vol%, and 6 vol%, respectively. The prepared precursor solution was dropped onto PEDOT: PSS and spin-coated at 4,500 rpm for 30 seconds. To create uniform and dense perovskite crystals, 150 μL of toluene (Fujifilm Wako Pure Chemical) was doped dropwise 10 seconds after the start of spin coating when KI is not doped. When KI is doped, 150 μL of toluene was doped dropwise 13 seconds after the start of spin coating. After that, annealing was performed on a hot plate at 100°C for 10 minutes.

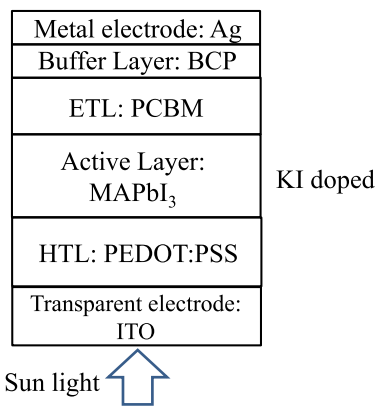

Fig. 1 Fabricated inversed-structured PSCs

[6,6]-Phenyl-C61-Butyric Acid Methyl [6,6]-Phenyl-C61-Butyric Acid Methyl Ester ($PC_{61}BM$) is used as the material of the electron transport layer. 20 mg of PCBM was dissolved in 1 mL of chlorobenzene (Fujifilm Wako Pure Chemical); after performing nitrogen substitution for 10 minutes in the glove box, it was stirred on a hot plate at 70°C for 12 hours with a stirrer at a rotation speed of 400 rpm. Before forming a film, filter through a filter with a filtration accuracy of 0.45 μm (Cytiva, 6872). Spin coat the filtered PCBM solution at 1,000 rpm for 30 seconds. Bathocuproine (BCP) (Kankohsya) was used as the material for the buffer layer. 0.5 mg of BCP was dissolved in 1 mL of ethanol (Fujifilm Wako Pure Chemical); after performing nitrogen substitution for 10 minutes in the glove box, it was stirred on a hot plate at 70°C for 12 hours with a stirrer at a rotation speed of 400 rpm. Then, the BCP solution is spin-coated at 3,000 rpm for 30 seconds. The metal electrode was produced by using a tungsten board (Plansee, SV07100) as the vapor deposition source for depositing silver using a thin-film deposition system (ULVAC, VTR-350/ERM). In film formation, silver is vaporized and deposited on the surface of the PCVs substrate by passing an electric current through the tungsten board and increasing the temperature. The deposition speed is controlled by the controller (ULVAC CRTM-9000G) to 0.2 nm/min.

The following measurements were used to measure the PVCs produced. A Simazu UV-2450 was used to measure the absorbance of the device, and a needle contact film thickness meter (Kosaka Laboratory Surfcorder ET200) was used to measure perovskite film thickness. The ionization potential was measured using an atmospheric photoelectron yield spectroscope (Riken Keiki AC-2) with a start energy 4.0 eV, end energy 6.5 eV, interval 0.05 eV, and light intensity 10 nW. The surface of the active layer was observed using an AFM (Keyence VN-8000). Rigaku RINT-2500 was used for X-ray analysis of the perovskite film surface, and the measurement was performed with Cu as a target, a voltage of 40 kV, a current of 100 mA, and a scan range of 5° to 60°. Current density–voltage (J–V) measurements were recorded by applying potential external biases to the cells and recording the output photocurrent with a digital source meter (Agilent B2901A). A 150-W xenon lamp (Bunkoukeiki Otento-SUN3Xe-S150) was used as the light source, and the output irradiation intensity was adjusted to the AM 1.5 G condition (100 mW/cm^2).

3. Results and Discussions

To investigate how the doped KI affects the perovskite layer, we measured the spectrum of perovskite crystals by ultraviolet visible photometer, measured the surface shape of perovskite by AFM, and analyzed the crystal structure by X-ray analysis. Figure 2 shows the spectrum from 650 nm to 900 nm wavelength when without KI dope, 3.0 vol%, and 6.0 vol% of KI is doped to the perovskite layer, respectively. In all wavelength regions, the absorbance increased in the order of 3.0 vol% of KI doped, 6.0 vol% of KI doped, and without KI. The film thickness was calculated from the absorbance at a wavelength of 700 nm; it was 0.604, 0.701, and 0.638, respectively, when KI was not doped, 3.0 vol% of KI doped, and 6.0 vol% of KI doped, respectively. The absorption ratio was 1 : 1.16 : 1.06, when it is 1 without KI. The perovskite film thickness measured by the needle contact film thickness meter was 396 nm, 365 nm, and 373 nm, respectively. The film thickness ratio was 1 : 0.922 : 0.942, when it is 1 without KI. Comparing the absorption ratio and film thickness ratio, it was 1.16 and 0.92 when 3 vol% of KI doped, and 1.06 and 0.942 when 6 vol% of KI doped, both of which had higher absorbance values with the dope of potassium. It is considered to be due to the increase in crystallinity and the amount of light absorbed by doping KI to the perovskite layer. Figure 3 shows the band gap calculated from Fig. 2 using the Tauc plot method [12]. The band gaps were 1.530 eV, 1.525 eV, and 1.525 eV when no KI doped, 3.0 vol% of KI doped, and 6.0 vol% of KI doped, respectively. As a result, it was confirmed that the band gap was narrowed by doping KI. Next, the ionization potentials of the perovskite solar cells without KI doped, with 3.0 vol% of KI doped, and with 6.0 vol% of KI doped were measured using an atmospheric photoelectron yield spectroscope. The results were −5.34 eV, −5.13 eV, and −5.13 eV, respectively. It was confirmed that the dope of KI shifts the top end of the valence band by 0.21 eV in the shallow direction. Figure 4 shows the energy band diagram obtained from the measurement results of the band gap and ionization potential calculated by the Tauc plot method in Fig. 3. By doping KI, the potential energy of the valence and conduction bands increased, as well as the band gap. In addition, the ionization potential of PEDOT: PSS as the hole transport layer and the absorption spectrum and ionization potential of PCBM as the electron transport layer were measured. Figure 5 shows the energy diagram of the PSCs to be fabricated. PSCs require a slight difference in the “energy positions of the top end valence band and the bottom end conduction band” of

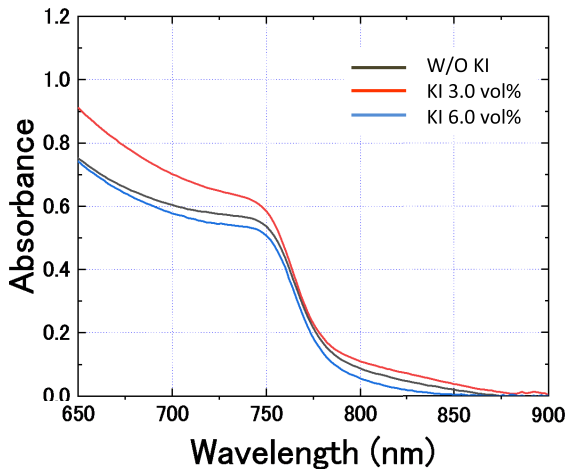

Fig. 2 Spectrum from 650 nm to 900 nm wavelength without KI, with 3.0 vol% KI, and with 6.0 vol% KI in the perovskite layer

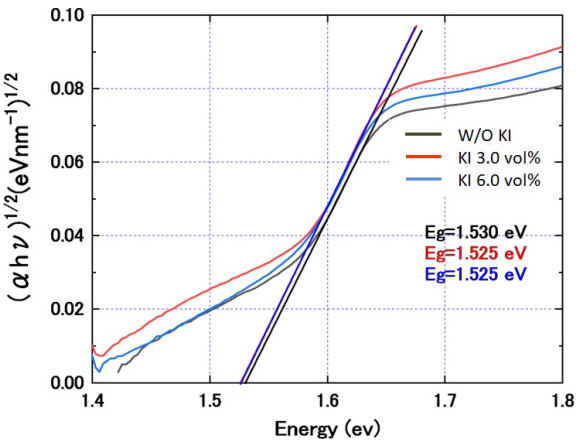

Fig. 3 Tauc plot from spectrum

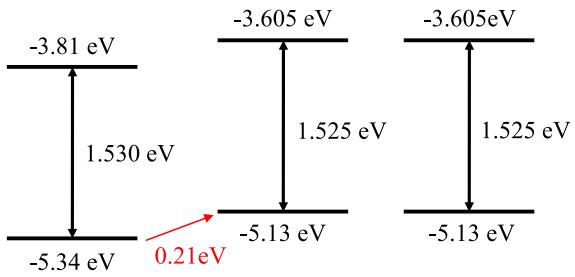

(a) W/O KI (b) KI 3.0 vol% and 6.0 vol%

Fig. 4 Energy band diagram of perovskite layer obtained from band gap and ionization potential measurements calculated by Tauc plot method

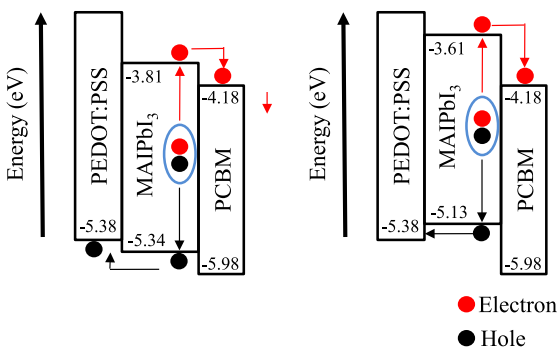

(a) W/O KI (b) KI 3.0 vol% and 6.0 vol%

Fig. 5 Energy diagrams of PSCs

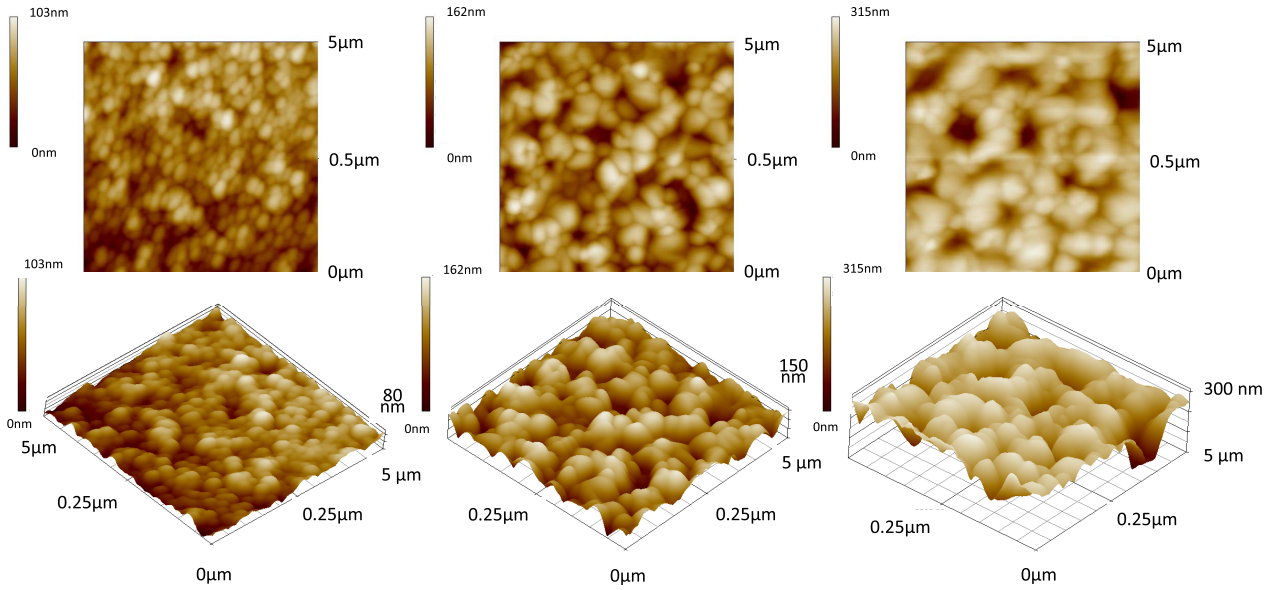

Fig. 6 AFM images of perovskite layer without KI, with 3.0 vol% KI, and with 6.0 vol% KI in the perovskite layer

the "carrier transport layer and the perovskite layer" to efficiently diffuse the generated carriers. It is also important to prevent backflow of carriers to improve the carrier transport efficiency. In the energy diagram without KI from Fig. 5, the difference in energy position at the top end of the valence band between PEDOT: PSS and the perovskite layer is 0.04 eV, and the difference between the perovskite layer and PCBM is 0.64 eV. The difference between the energy position at the bottom end of the conduction band between PCBM and the perovskite layer is 0.37 eV. In the energy diagrams when of the case with 3.0 vol% KI doped and 6.0 vol% of KI is doped, the difference in energy positions at the top end of the valence band between PEDOT: PSS and the perovskite layer is −0.25 eV, and the difference between the perovskite layer and PCBM is 0.85. The difference in the energy positions at the bottom end of the conduction band between PCBM and the perovskite layer is 0.58 eV. The energy positions at the top end of the valence band for KI3.0 vol% and KI6.0 vol% are shallower than the energy positions at the top end of the valence band for PEDOT: PSS, suggesting that hole transport is more difficult. In addition, the difference in the energy position at the bottom end of the conduction band between PCBM and the perovskite layer has increased from 0.25 eV to 0.58 eV, suggesting that the smoothness of electron transport has improved.

Figure 6 shows the AFM image of the perovskite layer without KI, with 3.0 vol% of KI doped, and with 6.0 vol% of KI doped, respectively in the perovskite layer. The scanning range of the AFM is 5 μm. The RMS values of root mean square surface roughness without KI, with 3.0 vol% of KI doped, and with 6.0 vol% of KI doped were 13.0 nm, 27.0 nm, and 48.4 nm, respectively. The KI-doped perovskite layer had pinholes. Pinholes cause an increase in leakage current due to increased parallel resistance in the equivalent circuit of the solar cell, and also hinder the transport of carriers. We believe that the main cause of the pinholes is the amount and timing of dropping toluene, the poor solvent, in addition to the difference in solvent engineering at the time of creation.

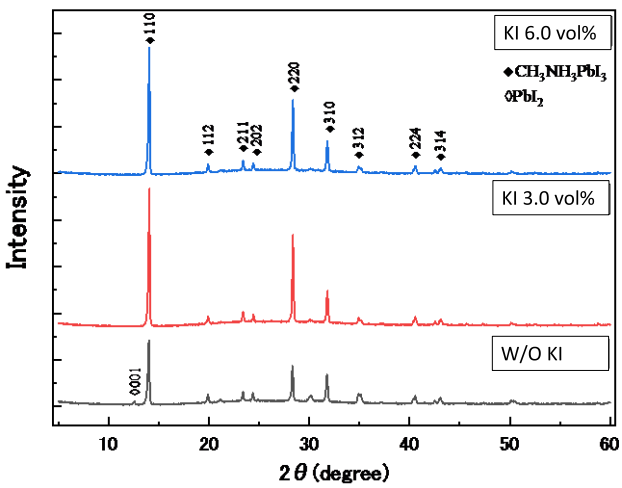

Fig. 7 XRD patterns of perovskite layer without KI, with 3.0 vol% KI, and with 6.0 vol% KI doped to the perovskite layer

Figure 7 shows the XRD pattern of the perovskite layer prepared with different KI dopes. In addition, the highest intensity was obtained from the 2θ = 14° (110) plane containing lead ions present in the body center of the perovskite crystal structure. A comparison was made between

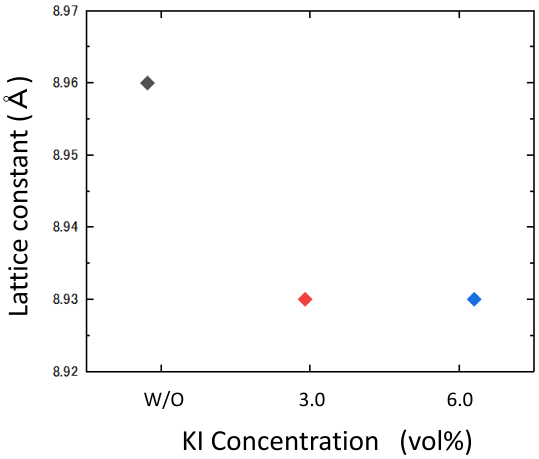

Fig. 8 Crystallinity calculated from XRD patterns without KI, with 3.0 vol% KI, and with 6.0 vol% KI doped to the perovskite layer

the peaks near $2\theta = 14°$ and the film thickness of the perovskite layer. From Fig. 7, the peak in the (001) plane indicating PbI_2 is shown in the case of no KI doped, and this peak disappears in the case of 3.0 vol% of KI doped and 6.0 vol% of KI doped. It is probable that the peak of PbI_2 (001) appeared due to the presence of unreacted PbI_2 because the amount of MAI was insufficient when the precursor solution was prepared. It is a crystal size calculated from XRD pattern of the perovskite layer prepared with KI dopes using Scherrer's formula [23]. It was calculated from the XRD peak intensity of 110 planes with the highest peak intensity. The crystal size without doping KI was 4.33 Å, the crystal size with 3.0 vol% KI was 5.13 Å, and the crystal size with 6.0 vol% KI was 5.17 Å.

Next, the crystallinity is calculated from the XRD patterns of the perovskite layers prepared with different KI dopes. The ratio of the peak area indicating the perovskite layer to the total peak area from $\theta = 5°$ to $60°$ is the crystallinity defined by Eq. (1).

$$C = \frac{A_{pc}}{A_T} \times 100 \quad (1)$$

Where C is Crystallinity, A_{pc} is total peak area of perovskite crystals, and A_T is total peak area. From Eq. (1), the crystallinity without KI doped was 35.8%, the crystallinity with 3.0 vol% of KI doped was 41.5%, and the crystallinity with 6.0 vol% of KI doped was 42.4%. As described above, the crystallinity increases as the KI dope increases. Figure 8 shows a comparison of the lattice constants calculated from the 110 planes with the highest peaks from the XRD patterns of the perovskite layers prepared with different KI dopes. From Fig. 8, it can be confirmed that the lattice constant is reduced by the dope of KI. The lattice constant is affected by the ionic radius of the materials that make up the crystal. The perovskite structure produced this time has a cubic structure, and MAI is contained in the A site of the perovskite crystal. MAI is the same monovalent cation as KI. The ionic radius of MAI is 2.70 Å, while the ionic radius of KI is 1.52 Å. The ionic radius of KI is smaller than the ionic

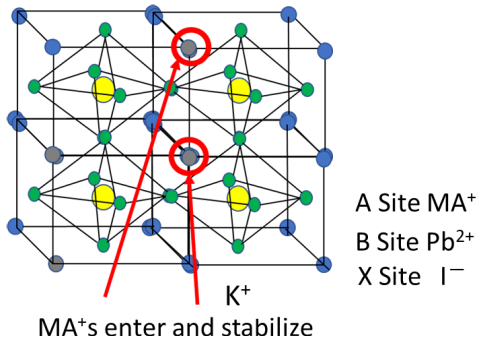

Fig. 9 Effect of KI dope on crystal structure

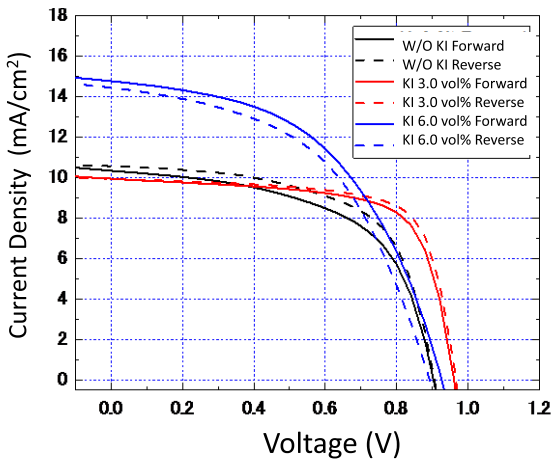

Fig. 10 J-V characteristics of perovskite solar cells fabricated with KI dopes at the highest PCE for each condition

radius of MAI. Therefore, it is considered that the lattice constant decreased as KI entered in place of MAI. Figure 9 is a schematic diagram of the effect of KI dope on the crystal structure. The decrease in the lattice constant indicates that a part of the A site is replaced from MAI to KI. Moreover, it is considered that stable and high-quality perovskite crystals are produced because the peak intensity and the crystallinity are improved.

Figure 10 shows the current density-voltage (J-V) characteristics at the highest PCE for each condition of perovskite solar cells fabricated with different KI dopes. Figure 11 shows a scatter plot of each parameter for 14 sheets of perovskite solar cells measured to confirm the variation. The mean value of J_{sc} was 7.29 mA/cm^2 without KI and the standard deviation was 1.850 mA/cm^2, the mean value of J_{sc} with 3.0 vol% of KI doped was 9.09 mA/cm^2 and the standard deviation was 1.277 mA/cm^2, and the mean value of J_{sc} with 6.0 vol% of KI doped was 11.36 mA/cm^2 and the standard deviation was 3.038 mA/cm^2. Statistical ANOVA confirmed that the difference between the population means of each J_{sc} was different 99% of the time. The mean value of V_{OC} without KI was 0.89 V and the standard deviation was 0.020 V, the mean value of V_{OC} with 3.0 vol% of KI doped was 0.92 V and the standard deviation was 0.067 V, and the mean value of V_{OC} with 6.0 vol% of KI doped was 0.90 V

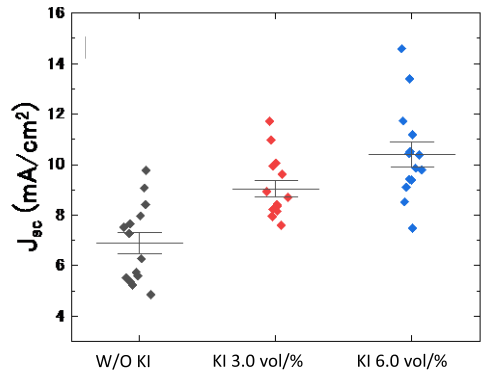

(a) J_{sc}

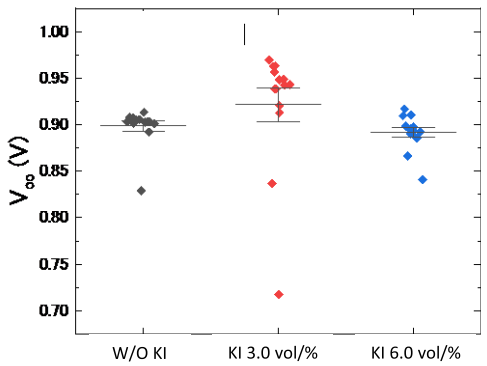

(b) V_{oc}

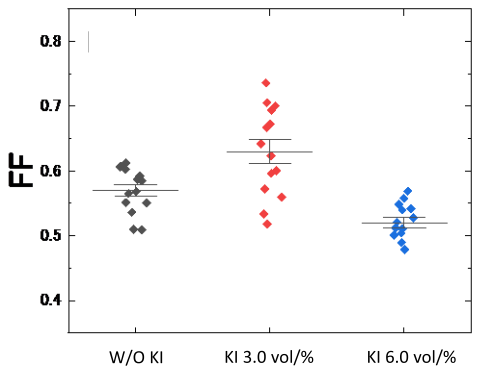

(c) FF

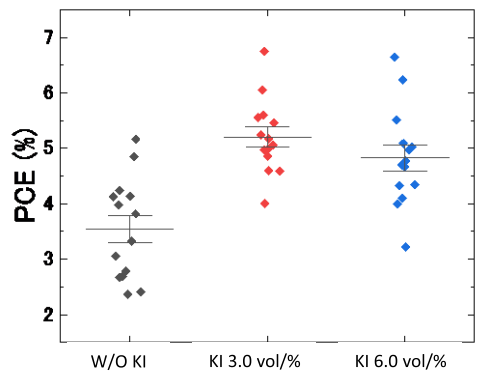

(d) PCE

Fig. 11 Scatter plots of each parameter of PSCs

and the standard deviation was 0.000 V. As a result of analysis of variance, it was confirmed that there was no difference between the population means of V_{OC}s 95% of the time. The mean value of FF without KI was 0.57 and the standard deviation was 0.001, the mean value of FF with 3.0 vol% of KI doped was 0.63 and the standard deviation was 0.005, and the mean value of FF with 6.0 vol% of KI doped was 0.52 and the standard deviation was 0.001. As a result of analysis of variance, it was confirmed that there is a 99% probability of difference in the population means of FF. The mean value of PCE without KI was 3.79% and the standard deviation was 1.091%, the mean value of PCE with 3.0 vol% of KI doped was 5.20% and the standard deviation was 0.673%, and the mean value of PCE with 6.0 vol% of KI doped was 5.20% and the standard deviation was 0.673%. As a result of analysis of variance, it was confirmed that there was a 99% probability of difference with and without KI, but there was no difference in 95% between KI 3.0 vol% and 6.0 vol%. From this result, it can be said that the dopes of KI increase Jsc and PCE. This is the same result as the perovskite solar cell with the sequential structure shown in the previous study [14]–[17].

4. Conclusion

In this report, the solar cell characteristics were evaluated by doping the power generation layer $MAPbI_3$ with 3.0 vol% and 6.0 vol% of KI in an inverse-structured perovskite solar cell. The Tauc plots of the absorbance characteristics and the ionization potential characteristics show that the top end of the valence band shifted by 0.21 eV in the shallow direction from −5.34 eV to −5.13 eV, and the energy band gap decreased from 1.530 eV to 1.525 eV. Also, the XRD measurements show that the lattice constant decreased from 8.96 Å to 8.93 Å when KI was doped. The decrease in the lattice constant indicates that a part of the A site is replaced from MAI to KI.

In the J-V characteristics of the solar cell, the mean value of J_{sc} improved from 7.0 mA/cm^2 without KI to 8.8 mA/cm^2 with 3.0 vol% of KI doped and to 10.2 mA/cm^2 with 6.0 vol% of KI doped. As a result, the mean value of PCE without KI was 3.5%, but the mean value of PCE improved to 5.2% with 3.0 vol% of KI doped and to 4.5% with 6.0 vol% of KI doped. Thus, it has shown that it is effective to dope KI to $MAIPBI_3$, which serves as the active layer, even in the inverse-structured PSCs.

Acknowledgments

This research was funded in part by the Science Research Promotion Fund and Aichi Institute of Technology Special Grant for Education and Research.

References

[1] A. Kojima, K. Teshima, Y. Shirai, and T. Miyasaka, "Organometal halide perovskites as visible-light sensitizers for photovoltaic cells,"

J. Am. Chem. Soc., vol.131, no.17, pp.6050–6051, 2009.
[2] J.-H. Im, C.-R. Lee, J.-W. Lee, S.-W. Park, and N.-G. Park, "6.5% efficient perovskite quantum-dot-sensitized solar cell," Nanoscale, vol.3, no.10, pp.4088–4093, 2011.
[3] P. Fan, D. Gu, G.-X. Liang, J.-T. Luo, J.-L. Chen, Z.-H. Zheng, and D.-P. Zhang, "High-performance perovskite $CH_3NH_3PbI_3$ thin films for solar cells prepared by single-source physical vapour deposition," Science reports, vol.6, 29910, 2016.
[4] S.D. Stranks, G.E. Eperon, G. Grancini, C. Menelaou, M.J.P. Alcocer, T. Leijtens, L.M. Herz, A. Petrozza, and H.J. Snaith, "Electron-Hole Diffusion Lengths Exceeding 1 Micrometer in an Organometal Trihalide Perovskite Absorber," Science, vol.342, no.6156, pp.341–344, 2013.
[5] V.O. Eze, Y. Seike, and T. Mori, "Synergistic Effect of Additive and Solvent Vapor Annealing on the Enhancement of $MAPbI_3$ Perovskite Solar Cells Fabricated in Ambient Air," ACS Applied Materials & Interfaces, vol.12, no.41, pp.46387–46845, 2020.
[6] D. Okawa, Y. Seike, and T. Mori, "Effect of 2-propanol Immersing on Organohalide Perovskite Layer in Perovskite Solar Cells Fabricated by Two-step Method," J. Photopoly. Sci. Tech., vol.34, no.3, pp.279–284, 2021.
[7] T. Mori, H. Okada, V.O. Eze, and Y. Seike, "Effect of Air-Flow and Solvent Annealing on Fabrication of Perovskite Active Layer and Photovoltaic Properties of Cells with the Active Layer," J. Photopoly. Sci. Tech., vol.33, no.4, pp.399–404, 2020.
[8] V.O. Eze, Y. Seike, and T. Mori, "Efficient planar perovskite solar cells using solution-processed amorphous WO_x /fullerene C60 as electron extraction layers," Organic Electronics, vol.46, pp.253–262, 2017.
[9] D.J. Lewis and P. O'Brien, "Ambient pressure aerosol-assisted chemical vapour deposition of (CH3NH3)PbBr3, an inorganic–organic perovskite important in photovoltaics," Chem. Commun., vol.50, pp.6319–6321, 2014.
[10] A. Mei, X. Li, L. Liu, Z. Ku, T. Liu, Y. Rong, M. Xu, M. Hu, J. Chen, Y. Yang, M. Grätzel, and H. Han, "A hole-conductor–free, fully printable mesoscopic perovskite solar cell with high stability" Science, vol.345, no.6194, pp.295–298, 2014.
[11] Information on: https://www.nrel.gov/pv/cell-efficiency.html
[12] S. Pang, H. Hu, J. Zhang, S. Lv, Y. Yu, F. Wei, T. Qin, H. Xu, Z. Liu, and G. Cui, "$NH_2CH{=}NH_2PbI_3$: An alternative organolead iodide perovskite sensitizer for mesoscopic solar cells," Chemistry of Materials, vol.26, no.3, pp.1485–1491, 2014.
[13] O.A. Syzgantseva, M. Saliba, M. Grätzel, and U. Rothlisberger, "Stabilization of the Perovskite Phase of Formamidinium Lead Triiodide by Methylammonium, Cs, and/or Rb Doping," J. Phys. Chem. Lett., vol.8, no.6, pp.1191–1196, 2017.
[14] Z. Tang, T. Bessho, F. Awai, T. Kinoshita, M.M. Maitani, R. Jono, T.N. Murakami, T.N. Murakami, H. Wang, T. Kubo, S. Uchida, and H. Segawa, "Hysteresis-free perovskite solar cells made of potassium-doped organometal halide perovskite," Scientific reports, vol.7, no.1, pp.1–7, 2017.
[15] J.K. Nam, S.U. Chai, W. Cha, Y.J. Choi, W. Kim, M.S. Jung, J. Kwon, D. Kim, and J.H. Park, "Potassium Incorporation for Enhanced Performance and Stability of Fully Inorganic Cesium Lead Halide Perovskite Solar Cells," Nano Lett., vol.17, no.3, pp.2028–2033, 2017.
[16] M. Zhang, J. Bing, Y. Cho, Y. Li, J. Zheng, C.F.J. Lau, M.A. Green, S. Huang, and A.W.Y. Ho-Baillie, "Synergistic effect of potassium and iodine from potassium triiodide complex additive on gas-quenched perovskite solar cells," Nano Energy, vol.63, 103853, pp.1–7, 2019.
[17] S. Kandori, T. Oku, K. Nishi, T. Kishimoto, N. Ueoka, and A. Suzuki, "Fabrication and characterization of potassiumand formamidinium-added perovskite solar cells," J. Ceram. Soc. Jpn., vol.128, no.10, pp.805–811, 2020.
[18] N.J. Jeon, J.H. Noh, Y.C. Kim, W.S. Yang, S. Ryu, S.I. Seok, "Solvent engineering for high-performance inorganic–organic hybrid perovskite solar cells," Nature Materials, vol.13, pp.897–903, 2014.
[19] J. Zhang, L. Zhang, X. Li, X. Zhu, J. Yu, K. Fan, "Binary Solvent Engineering for High-Performance Two-Dimensional Perovskite Solar Cells," ACS Sustainable Chem. Eng., vol.7, no.3, pp.3487–3495, 2019.
[20] L. Chao, T. Niu, W. Gao, C. Ran, L. Song, Y. Chen, and W. Huang, "Solvent Engineering of the Precursor Solution toward Large-Area Production of Perovskite Solar Cells," ACS Sustainable Chemistry & Engineering, vol.7, no.3, pp.3487–3495, 2019.
[21] R. Liu and K. Xu, "Solvent engineering for perovskite solar cells: a review," Micro & Nano Letters, vol.15, no.6, pp.349–353, 2020.
[22] J. Tauc, "Optical properties and electronic structure of amorphous Ge and Si," Materials Research Bulletin, vol.3, no.1, pp.37–46, 1968.
[23] P. Scherrer, "Bestimmung der Grösse und der innerenStruktur von Kolloidteilchen mittels Röntgenstrahlen, Nachrichten von der Gesellschaft der Wissenschaften, Göttingen," pp.98–100, 1918.
[24] A. Monshi, M.R. Foroughi, and M.R. Monshi, "Modified Scherrer Equation to Estimate More Accurately Nano-Crystallite Size Using XRD," World J. of Nano Sci. and Eng., vol.2, no.3, pp.154–160, 2012.

Tatsuya Kato received his MS in Engineering in 2022 from the Aichi Institute of Technology, Japan. He is currently an engineer at Nissan Automotive Technology CO., LTD. in Japan. His current work involves the design and development of battery management systems (BMS) for automotive e-power.

Yusuke Ichino is a Professor in Department of Electrical Engineering, Aichi Institute of Technology (AIT). He graduated from Nagoya University and obtained a PhD in 2004. He moved to AIT from Nagoya University in April 2020. His research interests include high-performance functional oxide materials including superconductors and organic thin-film solar cells.

Tatsuo Mori is a Professor in Department of Electrical Engineering, Aichi Institute of Technology (AIT). He graduated from Nagoya University and obtained a PhD in 1990. He moved to AIT from Nagoya University in April 2012. His research fields are the high field phenomenon of polymeric insulating materials and the fabrication and estimate of organic devices such as organic light-emitting-diode and organic photovoltaic cells.

Yoshiyuki Seike is an Active Professor at the Aichi Institute of Technology (AIT) Japan. He received his PhD in Science and Engineering (2009) from Saitama University and the MS (1993) and BS (1990) degree from Aichi Institute of Technology. From 1990–2016, he worked at Asahi Sunac Corporation. His field areas included organic material for photovoltaic cells, analysis of cleaning processes for semiconductor devices, and the ESD in semiconductor manufacturing.